

The Dynamics of the Rocking Frame

Nicos Makris and Michalis F. Vassiliou

Abstract This paper investigates the planar rocking response and stability analysis of an array of free-standing columns capped with a freely supported rigid beam. Part of the motivation for this study is the emerging seismic design concept of allowing framing systems to uplift and rock along their plane in order to limit bending moments and shear forces. Following a variational formulation the paper reaches the remarkable result that the dynamic rocking response of an array of free-standing columns capped with a rigid beam is identical to the rocking response of a single free-standing column with the same slenderness; yet with larger size—that is a more stable configuration. Most importantly, the study shows that the heavier the freely supported cap-beam is (epistyles with frieze atop), the more stable is the rocking frame, regardless of the rise of the center of gravity of the cap-beam; concluding that top-heavy rocking frames are more stable than when they are top-light. This “counter intuitive” finding renders rocking isolation a most attractive alternative for the seismic protection of bridges with tall piers.

Keywords Rocking isolation • Seismic protection • Ancient temples • Prefabricated bridges • Earthquake engineering

N. Makris (✉)

Department of Civil, Environmental and Construction Engineering,
University of Central Florida, Orlando, USA
e-mail: nicos.makris@ucf.edu; nmakris@upatras.gr

N. Makris

Department of Civil Engineering, University of Patras, Patras, Greece

M.F. Vassiliou

Institute of Structural Engineering (IBK), Swiss Federal Institute of Technology (ETHZ),
Zurich, Switzerland
e-mail: mfvassiliou@gmail.com

© Springer International Publishing Switzerland 2015

I.N. Psycharis et al. (eds.), *Seismic Assessment, Behavior and Retrofit of Heritage Buildings and Monuments*, Computational Methods in Applied Sciences 37, DOI 10.1007/978-3-319-16130-3_2

1 Introduction

The design of most modern structural framing systems is based on three basic concepts which are deeply rooted in structural engineering. The first concept is that of creating statically indeterminate (redundant) framing systems. When a “statically indeterminate” structure is subjected to strong lateral loads and some joints develop plastic hinges, there is enough redundancy in the system so that other joints maintain their integrity. The second concept, known as ductility, is the ability of the structure to maintain sufficient strength at large deformations. In this way, in the event of excessive lateral loads that may convert all joints into plastic hinges, the presence of a ductile behavior prevents collapse; however, in this case the structure may experience appreciable permanent displacements together with severe damage at the hinge zones. Therefore, in a strong earthquake, irreparable damage to structures is inevitable with this design philosophy. The third concept that dominates modern structural engineering is that of positive stiffness. When a structure behaves elastically, forces and deformations are proportional. When yielding is reached, the forces are no longer proportional to the deformations; however, in most cases the stiffness at any instant of the deformation history of the structure remains positive—that is if some force is needed to keep the structure away from equilibrium at some displacement; then a larger force is needed to keep the structure away from equilibrium at a larger displacement. Figure 1 (left) illustrates the deformation

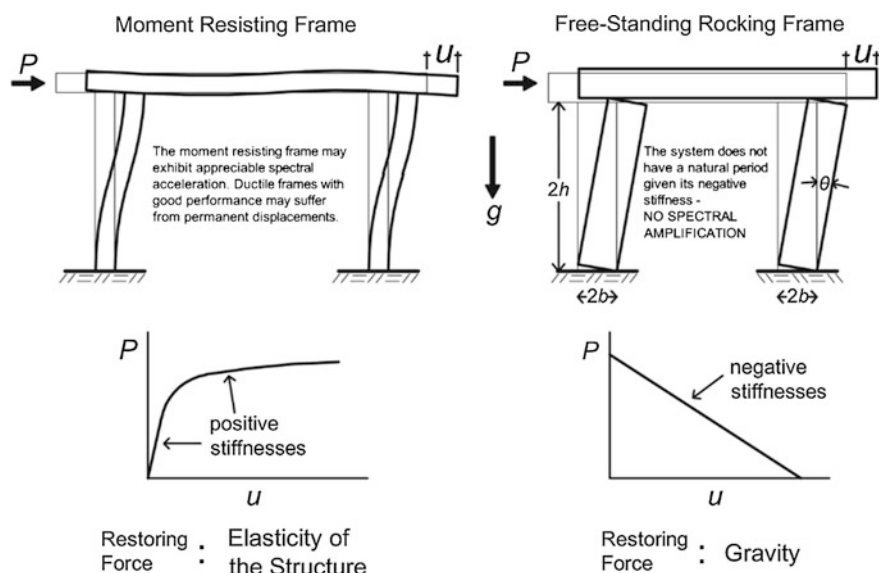


Fig. 1 The fundamental difference in the behavior of a traditional moment-resisting frame (left) and a rocking frame with free-standing columns which are allowed to rock (right)

pattern of a moment-resisting, fixed-base frame when subjected to a lateral load capable to induce yielding at the joints. The force-deformation curve (P - u) is nonlinear, the behavior is ductile; nevertheless, the lateral stiffness of the system remains positive at all times.

Next to the moment-resisting and ductile frame shown in Fig. 1 (left), Fig. 1 (right) illustrates the deformation pattern of a free-standing, rocking frame (two free-standing rigid columns capped with a freely supported rigid beam) when subjected to a lateral load capable to induce uplifting of the columns. The force-displacement relationship (P - u) of the rotating frame shown at the bottom of Fig. 1 (right) indicates that the articulated system has “infinite” stiffness until uplift is induced and, once the four-hinge frame is set into rocking motion its restoring force decreases monotonically, reaching zero when the rotation of the columns, $\theta = \alpha = \arctan(b/h)$.

Accordingly, the free-standing rocking frame shown in Fig. 1 (right) is a four-hinge mechanism that exhibits negative lateral stiffness. Furthermore, during the oscillatory rocking motion of a free-standing rocking frame, the force displacement curve does not enclose any area; therefore, the ductility of the system is zero, given that energy is lost only during impact when the angle of rotation reverses.

In summary, Fig. 1 indicates that, while most modern structural engineers are trained to design statically indeterminate and ductile structures that exhibit positive stiffness, ancient builders were designing entirely different structural systems—that is articulated mechanisms that exhibit marginal ductility and negative stiffness. What is remarkable about these “unconventional” articulated structures such as the



Fig. 2 View of the Temple of Aphaia, in Aegina, Greece. Its monolithic, free-standing columns support massive epistyles and the frieze atop and the entire rocking frame remains standing for more than 2500 years in a region with high seismicity

late archaic Temple of Aphaia in the island of Aegina nearby Athens (shown in Fig. 2) is that they have endured the test of time by surviving several strong seismic motions during their 2.5 millenia life.

Despite the documented remarkable seismic performance of the ancient articulated temples [3, 12, 19, 26, 31, 32, 37, 53], the number of modern structures that have been intentionally designed to rock on their foundations is limited [8]. Two state-of-the-practice examples may be found in New Zealand (a) the South Rangitikei Railway bridge [6] and (b) an industrial chimney at the Christchurch Airport [48]. Along the same concept is the design of the piers of the Rion–Antirion bridge in Greece [38].

Early studies on the seismic response of a slender rigid block were presented by Milne [34]; however, it was Housner [16] who uncovered a size-frequency scale effect which explained why: (a) the larger of two geometrically similar blocks can survive the excitation that will topple the smaller block; and (b) out of two same acceleration amplitude pulses, the one with the longer duration is more capable to induce overturning. Following Housner's seminal paper a number of studies have been presented to address the complex dynamics of one of the simplest man-made structures—the free standing rigid column.

Yim et al. [57] conducted numerical studies by adopting a probabilistic approach, Aslam et al. [5] confirmed with experimental studies that the rocking response of rigid blocks is sensitive to system parameters; while Psycharis and Jennings [39] examined the uplift of rigid bodies supported on viscoelastic foundation. Subsequent studies by Spanos and Koh [49] investigated the rocking response due to harmonic steady-state loading and identified “safe” and “unsafe” regions together with the fundamental and suharmonic modes of the system. Their study was extended by [14, 15] who further elucidated the mathematical structure of the problem by introducing the concepts of orbital stability and Poincare sections. The transient rocking response of free-standing rigid blocks was examined in depth by Zhang and Makris [58] who showed that there exist two modes of overturning: (a) by exhibiting one or more impacts; and (b) without exhibiting any impact. The existence of the second mode of overturning results in a safe region that is located on the acceleration-frequency plane above the minimum overturning acceleration spectrum. The fundamental differences between the response of a rocking rigid column (inverted pendulum) and the response of the linear elastic oscillator (regular pendulum) led to the development of the rocking spectrum [26]. More recent studies pertinent to the rocking response of rigid columns have focused on more practical issues such as representation of the impact [40], the effect of the flexibility-yielding of the supporting base [4, 35, 36] or the effect of seismic isolation [53]. Acikgoz and DeJong [1] and Vassiliou et al. [54] conducted analytical studies on the rocking response of elastic columns, while Truniger et al. [50] presented recently experimental results.

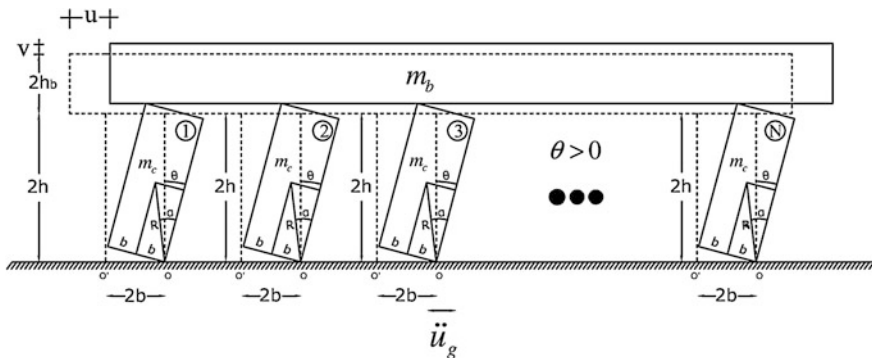


Fig. 3 Rocking array of free-standing columns capped with a freely supported rigid beam

In this paper we investigate the planar rocking response of an array of free-standing columns capped with a freely supported rigid beam as shown schematically in Fig. 3. Herein we use the term “rocking frame” for the one degree of freedom structure shown in Fig. 3. Sliding does not occur either at the pivot points at the base or at the pivot points at the cap-beam.

Our interest to this problem was partly motivated from the need to explain the remarkable seismic stability of ancient free-standing columns which support heavy free standing epistyles together with the even heavier frieze atop. As an example, Fig. 2 shows the entrance view of the late archaic Temple of Aphaia in the island of Aegina nearby Athens, Greece. Dates ranging from 510BC to 470BC have been proposed for this temple. All but three of the 32 outer columns of the temple are monolithic and they have been supporting for 2.5 millennia the front and back epistyles together with the heavy frieze (triglyph and metope). In ancient Greek temples the epistyles are positioned from the vertical axis of one column to the vertical axis of the neighboring column; therefore, the joint of the epistyles are along the vertical axis of the column (see Fig. 2). With this configuration during lateral loading of the peristyle of the temple, each epistyle in addition to the horizontal translation, u , shown in Fig. 3 it will also experience a small rotation, while the transfer of forces from the epistyles to the columns is not concentrated at the top pivoting point of the columns. Accordingly, the planar rocking response of the peristyle of ancient temples is more complicated than the planar motion of the idealization shown in Fig. 3.

Nevertheless; the striking dynamic stability of these monuments is mainly due to the development of rocking mechanisms. Motivated from this outstanding performance, this paper examines the dynamic response and stability of the simplest free-standing rocking frame shown in Fig. 3 in an effort to understand the dynamics of this nonlinear articulated structure.

The understanding of the rocking response and stability of the configuration shown in Fig. 3 is also pertinent to the growing precast bridge construction technology where bridge piers supporting heavy decks are allowed to rock atop their foundation in order to achieve re-centering of the bridge bent after a seismic event.

2 A Notable Limitation of the Equivalent Static Lateral Force Analysis

2.1 Seismic Resistance of Free-Standing Columns Under “Equivalent Static” Lateral Loads

Consider a free-standing rigid column with size $R = \sqrt{b^2 + h^2}$ and slenderness $b/h = \tan \alpha$ as shown in Fig. 4 (left). Let us first assume that the base of the column is moving (say to the left) with a “slowly” increasing acceleration, \ddot{u}_g (say a very long-duration acceleration pulse which allows for an equivalent static analysis). Uplift of the block (hinge formation) happens when the seismic demand (overturning moment) $= m\ddot{u}_g h$ reaches the seismic resistance (recentering moment) $= mgb$. When uplifting is imminent, “static” moment equilibrium of the block about the pivoting point O gives

$$\underbrace{m\ddot{u}_g h}_{\text{demand}} = \underbrace{mgb}_{\text{resistance}} \quad \text{or} \quad \underbrace{\ddot{u}_g}_{\text{demand}} = g \frac{b}{h} = \underbrace{g \tan \alpha}_{\text{resistance}} \quad (1)$$

Equation 1, also known as West’s formula [18, 34], shows that the block $\langle b, h \rangle$ will uplift when $\ddot{u}_g \geq g \tan \alpha$. Now, given that this is a “quasi-static” lateral inertial loading, the inertia moment due to the nearly zero rotational accelerations of the blocks is negligible ($\ddot{\theta}(t) = 0$). Upon uplift has occurred, the rocking block

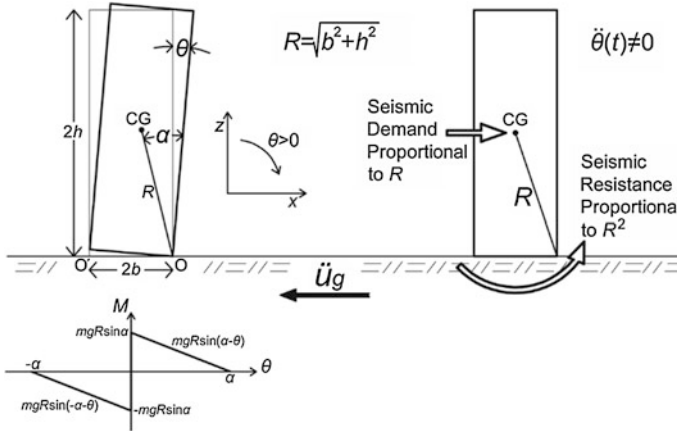


Fig. 4 *Left* Geometric characteristics of a free-standing rocking column together with its moment rotation diagram. *Right* During earthquake shaking which sets the column in rocking motion ($\ddot{\theta}(t) \neq 0$) the seismic resistance is proportional to R^2 ; while, the seismic demand is proportional to R . Consequently, when a free-standing column is sufficiently large it can survive large horizontal accelerations even if it is very slender

experiences a positive rotation, $\theta(t)$; therefore, the seismic demand is $m\ddot{u}_g R \cos(\alpha - \theta(t))$; while the seismic resistance is merely $mgR \sin(\alpha - \theta(t))$ since $\ddot{\theta}(t) = 0$. For $\theta > 0$, the resistance of the rocking block upon uplifting under quasi-static lateral loading is $\tan(\alpha - \theta(t))$ which is smaller than $\tan \alpha$. Accordingly; once the block uplifts, it will also overturn. From this analysis one concludes that under quasi-static lateral loading the stability of a free-standing column depends solely on its slenderness ($g \tan \alpha$) and is independent to the size ($R = \sqrt{b^2 + h^2}$).

2.2 Seismic Resistance of Free-Standing Columns Subjected to Dynamic Loads

In reality, earthquake shaking, \ddot{u}_g , is not a quasistatic loading and upon uplifting has occurred the block will experience a finite rotational acceleration ($\ddot{\theta}(t) \neq 0$). In this case, dynamic moment equilibrium gives

$$\underbrace{-m\ddot{u}_g(t)R \cos[\alpha - \theta(t)]}_{\text{seismic demand}} = \underbrace{I_o \ddot{\theta}(t) + mgR \sin[\alpha - \theta(t)]}_{\text{seismic resistance}}, \quad \theta > 0 \quad (2)$$

where I_o is the rotational moment of inertia of the column about the pivot point at the base—a quantity that is proportional to the square of the size of the column R . As an example for rectangular columns, $I_o = \frac{4}{3}mR^2$, and Eq. 2 simplifies to

$$\underbrace{-\ddot{u}_g(t)R \cos[\alpha - \theta(t)]}_{\text{seismic demand}} = \underbrace{\frac{4}{3}R^2 \ddot{\theta}(t) + gR \sin[\alpha - \theta(t)]}_{\text{seismic resistance}}, \quad \theta > 0 \quad (3)$$

Equation 3 indicates that when a slender free-standing column is set into rocking motion the seismic demand (overturning seismic moment) is proportional to R (first power of the size); whereas, the seismic resistance (opposition to rocking) is proportional to R^2 (second power of the size). Consequently, Eq. 3 dictates that regardless how slender a column is (small α) and how intense the ground shaking, \ddot{u}_g , is (large seismic demand), when a rotating column ($\ddot{\theta}(t) = \text{finite}$) is large enough, the second power of R in the right-hand-side (seismic resistance) can always ensure stability. Simply stated, Housner's [16] size-frequency effect is merely a reminder that a quadratic term eventually dominates over a linear term regardless the values of their individual coefficients [22].

Figure 4 (right) shows schematically the relations with the size R of the seismic demand (linear relation) and the seismic resistance (quadratic relation). From its very conception the “equivalent static lateral force analysis” is not meant to deal

with any rotational acceleration term; therefore, its notable failure to capture the seismic stability (resistance) of tall free-standing structures.

For negative rotations ($\theta(t) < 0$), the equation of motion of a rocking block is

$$-m\ddot{u}_g(t)R \cos[-\alpha - \theta(t)] = I_o\ddot{\theta}(t) + mgR \sin[-\alpha - \theta(t)], \quad \theta < 0 \quad (4)$$

Equations 2 and 4 are well known in literature ([24, 30, 57, 58] and references reported therein) and are valid for arbitrary values of the slenderness angle $\alpha = \arctan(b/h)$. Equations 2 and 4 can be expressed in the compact form

$$\ddot{\theta}(t) = -p^2 \left\{ \sin[\alpha \operatorname{sgn}[\theta(t)] - \theta(t)] + \frac{\ddot{u}_g}{g} \cos[\alpha \operatorname{sgn}[\theta(t)] - \theta(t)] \right\}. \quad (5)$$

In Eq. 5, the quantity $p = \sqrt{mRg/I_o}$ is the frequency parameter of the block and is an expression of its size. For rectangular blocks $p = \sqrt{3g/(4R)}$.

Figure 4 (left) shows the moment-rotation relationship during the rocking motion of a free-standing block. The system has infinite stiffness until the magnitude of the applied moment reaches the value $mgR \sin \alpha$, and once the block is rocking, its restoring force decreases monotonically, reaching zero when $\theta = \alpha$. This negative stiffness, which is inherent in rocking systems, is most attractive in earthquake engineering in terms of keeping base shears and moments low [26], provided that the rocking block remains stable, thus the need for a formulae that will offer a safe design value for its slenderness.

During the oscillatory motion, the moment-rotation curve follows the curve shown in Fig. 3 without enclosing any area. Energy is lost only during impact, when the angle of rotation reverses. The ratio of kinetic energy after and before impact is

$$r = \frac{\dot{\theta}_2^2}{\dot{\theta}_1^2} \quad (6)$$

which means that the angular velocity after the impact is only \sqrt{r} times the velocity before the impact. Substitution of Eq. 4 into Eq. 5 gives

$$r = \left[1 - \frac{3}{2} \sin^2 \alpha \right]^2 \quad (7)$$

The value of the coefficient of restitution given by Eq. 6 is the maximum value of r under which a free-standing rigid block with slenderness α will undergo rocking motion. Consequently, in order to observe rocking motion, the impact has to be inelastic. The less slender a block (larger α), the more plastic is the impact, and for the value of $\alpha = \sin^{-1} \sqrt{2/3} = 54.73^\circ$, the impact is perfectly plastic.

During the rocking motion of slender blocks, if additional energy is lost due to the inelastic behavior at the instant of impact, the value of the true coefficient of restitution r will be less than the one computed from Eq. 6.

3 Equation of Motion of the Rocking Frame

The free standing rocking frame shown in Fig. 3 is a single-degree-of-freedom structure with size $R = \sqrt{h^2 + b^2}$ and slenderness $\alpha = a \tan(b/h)$. The only other parameter that influences the dynamics of the rocking frame is the ratio of the mass of the cap-beam, m_b , to the mass of all the N rocking columns, m_c , $\gamma = \frac{m_b}{Nm_c}$. For the temple of Apollo in Corinth where the frieze is missing, γ is as low as 0.3; whereas in prefabricated bridges $\gamma > 4$. As in the case of the single rocking column, the coefficient of friction is large enough so that sliding does not occur at the pivot point at the base and at the cap-beam. Accordingly, the horizontal translation displacement $u(t)$ and the vertical lift $v(t)$ of the cap-beam are functions of the single degree of freedom $\theta(t)$. For a positive horizontal ground acceleration (the ground is accelerating to the right), the rocking frame will initially rock to the left ($\theta(t) < 0$). Assuming that the rocking frame will not topple, it will recenter, impacts will happen at the pivot points (at the base and at the cap-beam) and subsequently it will rock to the right ($\theta(t) > 0$). During rocking the dependent variables $u(t)$, $v(t)$ and their time derivatives are given for $\theta(t) < 0$ and $\theta(t) > 0$ by the following expressions.

$$u = \mp 2R(\sin \alpha - \sin(\alpha \pm \theta)) \quad (8)$$

$$\dot{u} = 2R \cos(\alpha \pm \theta) \dot{\theta} \quad (9)$$

$$\ddot{u} = 2R \left(\mp \sin(\alpha \pm \theta) (\dot{\theta})^2 - \cos(\alpha \pm \theta) \ddot{\theta} \right) \quad (10)$$

and

$$v = 2R(\cos(\alpha \pm \theta) - \cos \alpha) \quad (11)$$

$$\dot{v} = \mp 2R \sin(\alpha \pm \theta) \dot{\theta} \quad (12)$$

$$\ddot{v} = -2R \left(\cos(\alpha \pm \theta) (\dot{\theta})^2 + \sin(\alpha \pm \theta) \ddot{\theta} \right) \quad (13)$$

In the equations above, whenever there is a double sign (say \pm) the top sign is for $\theta(t) < 0$ and the bottom sign is for $\theta(t) > 0$.

During rocking motion Langrange's equation must be satisfied,

$$\frac{d}{dt} \left(\frac{dT}{d\dot{\theta}} \right) - \frac{dT}{d\theta} = Q. \quad (14)$$

In Eq. 13, T is the kinetic energy of the system and Q is the generalized force acting on the system

$$Q = - \frac{dW}{d\theta} \quad (15)$$

in which W is the work done by the external forces acting on the rocking frame during an admissible rotation $\delta\theta$. During this admissible rotation $\delta\theta$, the variation of work is

$$\delta W = \frac{dW}{d\theta} \delta\theta \quad (16)$$

In either case were $\theta(t) < 0$ or $\theta(t) > 0$ the kinetic energy of the system is

$$T = N \frac{1}{2} I_o (\dot{\theta})^2 + \frac{1}{2} m_b ((\dot{u})^2 + (\dot{v})^2) \quad (17)$$

Using Eqs. 8, 11 and 16 reduces to

$$T = \left(\frac{N}{2} I_o + 2m_b R^2 \right) (\dot{\theta})^2 \quad (18)$$

Our analysis proceeds by first investigating the rocking motion of a free-standing frame subjected to a horizontal ground acceleration $\ddot{u}_g(t)$ when $\theta(t) < 0$. During this segment of the motion the variation of the work, W , is

$$\delta W = \left(m_b + \frac{N}{2} m_c \right) (\ddot{u}_g \delta u + g \delta v) \quad (19)$$

The combination of Eqs. 15 and 19 gives

$$\frac{dW}{d\theta} = \left(m_b + \frac{N}{2} m_c \right) \left(\ddot{u}_g \frac{du}{d\theta} + g \frac{dv}{d\theta} \right) \quad (20)$$

which simplifies to

$$\frac{dW}{d\theta} = 2R \left(m_b + \frac{N}{2} m_c \right) (\ddot{u}_g \cos(\alpha + \theta) - g \sin(\alpha + \theta)) \quad (21)$$

after using the expression given by Eqs. 8 and 11.

The substitution of Eqs. 17 and 21 into Lagrange's equation given by Eq. 14 results to the equation of motion of the rocking frame for $\theta(t) < 0$.

$$\frac{\frac{I_o}{2m_c R} + 2\gamma R}{(\gamma + \frac{1}{2})g} \ddot{\theta} = \sin(\alpha + \theta) - \frac{\ddot{u}_g}{g} \cos(\alpha + \theta) \quad (22)$$

where $\gamma = \frac{m_b}{Nm_c}$ is the ratio of the mass of the cap-beam (epistyle), m_b , to the imass of all the N columns $= Nm_c$.

For the case where the rotation is positive $\theta(t) > 0$ the variation of the work is

$$\delta W = \left(m_b + \frac{N}{2} m_c \right) (\ddot{u}_g \delta u + g \delta v) \quad (23)$$

and Eq. 16 takes the form

$$\frac{dW}{d\theta} = 2R \left(m_b + \frac{N}{2} m_c \right) (\ddot{u}_g \cos(\alpha - \theta) + g \sin(\alpha - \theta)) \quad (24)$$

The substitution of Eqs. 17 and 24 into Lagrange's equation given by Eq. 13 offers the equation of motion of the rocking frame for $\theta(t) > 0$.

$$\frac{\frac{I_o}{2m_c R} + 2\gamma R}{(\gamma + \frac{1}{2})g} \ddot{\theta} = -\sin(\alpha - \theta) - \frac{\ddot{u}_g}{g} \cos(\alpha - \theta). \quad (25)$$

For rectangular columns $I_o = (4/3)mR^2$; and Eqs. 22 and 25 can be expressed in a single compact form

$$\ddot{\theta} = -\frac{1+2\gamma}{1+3\gamma} p^2 \left(\sin[\text{asgn}(\theta(t)) - \theta(t)] + \frac{\ddot{u}_g(t)}{g} \cos[\text{asgn}(\theta(t)) - \theta(t)] \right) \quad (26)$$

Equation 26 which describes the planar motion of the free-standing rocking frame is precisely the same as Eq. 3 which describes the planar rocking motion of a single free-standing rigid column with the same slenderness α , except that in the rocking frame the term p^2 is multiplied with the factor $\frac{1+2\gamma}{1+3\gamma}$. Accordingly, the frequency parameter of the rocking frame, \hat{p} , is

$$\hat{p} = \sqrt{\frac{1+2\gamma}{1+3\gamma}} p \quad (27)$$

where $p = \sqrt{\frac{3g}{4R}}$ is the frequency parameter of the solitary rocking column and $\gamma = \frac{m_b}{Nm_c}$ is the mass of the cap-beam to the mass of all N columns.

For a light cap-beam ($\gamma = \frac{m_b}{Nm_c} \rightarrow 0$), the multiplication factor $\frac{1+2\gamma}{1+3\gamma} \rightarrow 1$ and the array of free standing columns coupled with a light epistyle exhibit precisely the dynamic rocking response of the solitary free-standing column. On the other hand, as the mass of the epistyle increases

$$\lim_{\gamma \rightarrow \infty} \frac{1+2\gamma}{1+3\gamma} = \frac{2}{3}. \quad (28)$$

Accordingly, the dynamic behavior of a rocking frame with a very heavy cap-beam supported on columns with slenderness α and frequency parameter, $p = \sqrt{\frac{3g}{4R}}$, is identical to the dynamic rocking response of a single rigid column with slenderness α and frequency parameter $\hat{p} = \sqrt{\frac{2}{3}}p$ —that is a smaller frequency parameter; therefore a larger, more stable column.

This remarkable result offered by Eq. 26—that the heavier the cap-beam is, the more stable is the free standing rocking frame despite the rise of the center of gravity of the cap-beam—has been also confirmed by obtaining Eq. 26 for a pair of columns with the algebraically-intense direct formulation after deriving the equations of motion of the two-column frame through dynamic equilibrium. Furthermore, numerical studies with the discrete element method (DEM) by Papaloizou and Komodromos [37] concluded to the same result—that the planar response of free-standing columns supporting epistyles is more stable than the response of the solitary, free-standing column.

According to Eq. 26 the rocking response and stability analysis of the free-standing rocking frame with columns having slenderness, α , and size R , is described by all the past published work on the rocking response of the free-standing single block ([5, 16, 26, 49, 53, 57, 58] among others), where the block has the same slenderness, α , and a larger size \hat{R} given by

$$\hat{R} = \frac{1+3\gamma}{1+2\gamma}R = \left(1 + \frac{\gamma}{1+2\gamma}\right)R \quad (29)$$

When replacing the rocking frame with the larger-size, equal slenderness solitary column, the maximum coefficient of restitution is given by Makris and Vassiliou [31].

$$r = \left(\frac{\dot{\theta}_2}{\dot{\theta}_1}\right)^2 = \left(\frac{1 - \frac{3}{2}\sin^2 \alpha + 3\gamma \cos 2\alpha}{1+3\gamma}\right)^2 \quad (30)$$

4 Overturning Spectra—Self Similar Response for Pulselike Excitations

The relative simple form yet destructive potential of near source ground motions has motivated the development of various closed form expressions which approximate their dominant kinematic characteristics. The early work of Veletsos et al. [55] was followed by the papers of Hall et al. [13], Makris [21], Makris and Chang [23], Alavi and Krawinkler [2] and more recently by the papers of Mavroeidis and Papageorgiou [33] and Vassiliou and Makris [51, 52]. Physically realizable pulses can adequately describe the impulsive character of near-fault ground motions both qualitatively and quantitatively. The minimum number of parameters of the mathematical pulse is two, which are the acceleration amplitude, a_p and the duration T_p . The more sophisticated model of Mavroeidis and Papageorgiou [33] involves 4 parameters which are the pulse period, the pulse amplitude, the pulse phase and the number of half cycles. Recently, Vassiliou and Makris [51, 52] used the Mavroeidis and Papageorgiou model [33] in association with wavelet analysis to develop a mathematically formal and objective procedure to extract the time scale and length scale of strong ground motions.

The current established methodologies for estimating the pulse characteristics of a wide class of records are of unique value, since the product, $a_p T_p^2 = L_p$ is a characteristic length scale of the ground excitation and is a measure of the persistence of the most energetic pulse to generate inelastic deformation [27, 28]. It is emphasized that the persistence of the pulse, $a_p T_p^2 = L_p$, is a different characteristic than the strength of the pulse which is measured with the peak pulse acceleration, a_p . The reader may recall that among two pulses with different acceleration amplitudes (say $a_{p1} > a_{p2}$) and different pulse durations (say $T_{p1} < T_{p2}$) the inelastic deformation does not scale with the peak pulse acceleration (most intense pulse) but with the strongest length scale (larger $a_p T_p^2 =$ most persistent pulse), [17, 27, 28].

The heavy dark line in Fig. 5 (Top) which approximates the long-period acceleration pulse of the NS component of the 1992 Erzincan, Turkey, record is a scaled expression of the second derivative of the Gaussian distribution, $e^{-t^2/2}$, known in the seismological literature as the symmetric Ricker wavelet [41, 42].

$$\psi(t) = a_p \left(1 - \frac{2\pi^2 t^2}{T_p^2}\right) e^{-\frac{1}{2} \frac{2\pi^2 t^2}{T_p^2}} \quad (31)$$

The value of $T_p = \frac{2\pi}{\omega_p}$, is the period that maximizes the Fourier spectrum of the symmetric Ricker wavelet. Similarly, the heavy dark line in Fig. 5 (Bottom) which approximates the long-period acceleration pulse of the Pacoima Dam motion recorded during the February 9, 1971 San Fernando, California earthquake is a scaled expression of the third derivative of the Gaussian distribution $e^{-\frac{t^2}{2}}$.

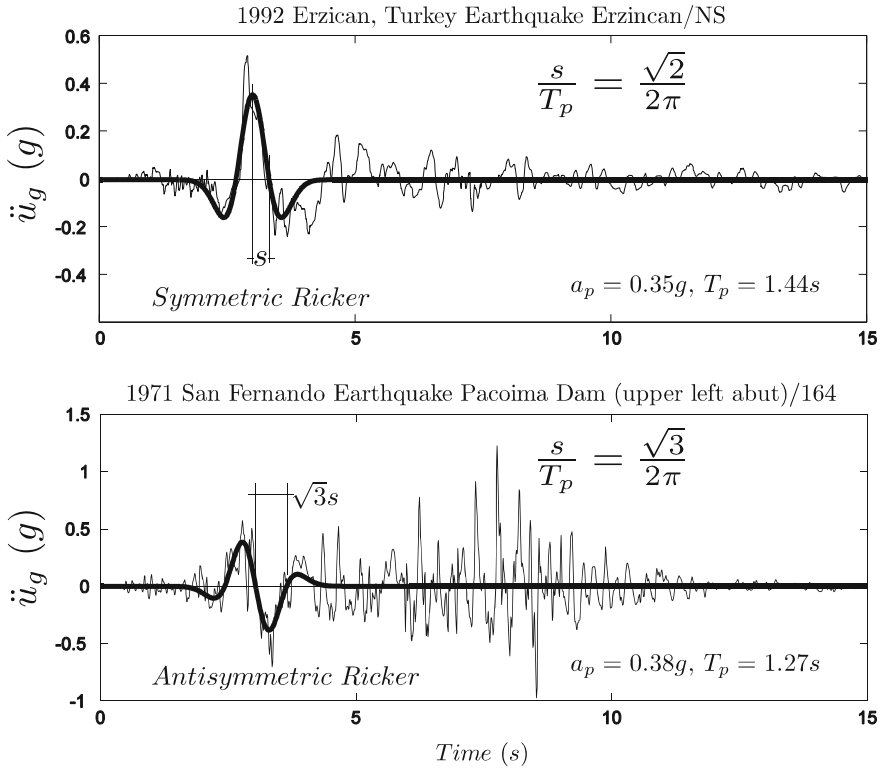


Fig. 5 *Top* North-South components of the acceleration time history recorded during the 1992 Erzican, Turkey earthquake together with a symmetric Ricker wavelet. *Bottom* Fault-normal component of the acceleration time history recorded during the 1971 San Fernando earthquake, together with an antisymmetric Ricker wavelet

$$\psi(t) = \frac{a_p}{\beta} \left(\frac{4\pi^2 t^2}{3T_p^2} - 3 \right) \frac{2\pi t}{\sqrt{3}T_p} e^{-\frac{14\pi^2 t^2}{2 \cdot 3T_p^2}} \quad (32)$$

in which β is a factor equal to 1.3801 that enforces the above function to have a maximum equal to a_p .

The choice of the specific functional expression to approximate the main pulse of pulse-type ground motions has limited significance in this work. What is important to recognize is that several strong ground motions contain a distinguishable acceleration pulse which is responsible for most of the inelastic deformation of structures ([2, 13, 17, 23, 29] among others). A mathematically rigorous and easily reproducible methodology based on wavelet analysis to construct the best matching wavelet has been recently proposed by Vassiliou and Makris [52].

Consider the free-standing rocking frame shown in Fig. 2 that is subjected to an acceleration pulse (like those shown in Fig. 5) with acceleration amplitude a_p and pulse duration, $T_p = \frac{2\pi}{\omega_p}$. From Eq. 26 it results that the response of a free-standing rocking frame subjected to an acceleration pulse is a function of six variables

$$\theta(t) = f(p, \alpha, \gamma, g, a_p, \omega_p) \quad (33)$$

The seven variables appearing in Eq. 33 involve only two reference dimensions; that of length [L] and time [T]. According to Buckingham's Π -Theorem, the number of dimensionless products with which the problem can be completely described is equal to [number of variables = 7] – [number of reference dimensions = 2] = 5. Herein we select as repeating variables the characteristics of the pulse-excitation, a_p and ω_p and the five independent Π -products are: $\Pi_\theta = \theta$, $\Pi_\omega = \omega_p/p$, $\Pi_\alpha = \tan \alpha$, $\Pi_\gamma = \gamma$ and $\Pi_g = a_p/g$. With these five dimensionless Π -products, Eq. 33 reduces to

$$\theta(t) = \varphi\left(\frac{\omega_p}{p}, \tan \alpha, \gamma, \frac{a_p}{g}\right) \quad (34)$$

The rocking response of the free-standing frame shown in Fig. 2 when subjected to a horizontal base acceleration history $\ddot{u}_g(t)$ is computed by solving Eq. 26 in association with the minimum energy loss expression given by Eq. 30 which takes place at every impact.

Figure 6 shows the minimum overturning acceleration spectra of a free-standing rocking frame when subjected to a symmetric Ricker pulse (left) and an antisymmetric Ricker pulse (right) for different values of the mass ratio $\gamma = \frac{m_b}{Nm_c}$. The top plots are for values of the column slenderness $\alpha = 10^\circ$ and the bottom plots are for $\alpha = 14^\circ$.

In constructing Fig. 6, the frequency parameter p is the frequency parameter of the columns of the frame (not \hat{p}) and the enhanced stability of the rocking frame due to (a) the corresponding larger size, $\hat{p} = \sqrt{\frac{1+2\gamma}{1+3\gamma}}p$, and (b) the reduced coefficient of restitution (see Eq. 30) is given by the curves for each given value of γ .

Figure 6 indicates that up to values of $\omega_p/p = 4$ the additional stability of the rocking frame versus the stability of the equal slenderness solitary column is marginal.

For values of $\omega_p/p > 4$ (larger columns or shorter period pulses) the minimum acceleration overturning spectra of the rocking frame are higher than the corresponding spectrum of the solitary rocking column showing the enhanced seismic stability of the top-heavy rocking frame. This enhanced seismic stability is indifferent to the height of the center of gravity of the cap-beam.

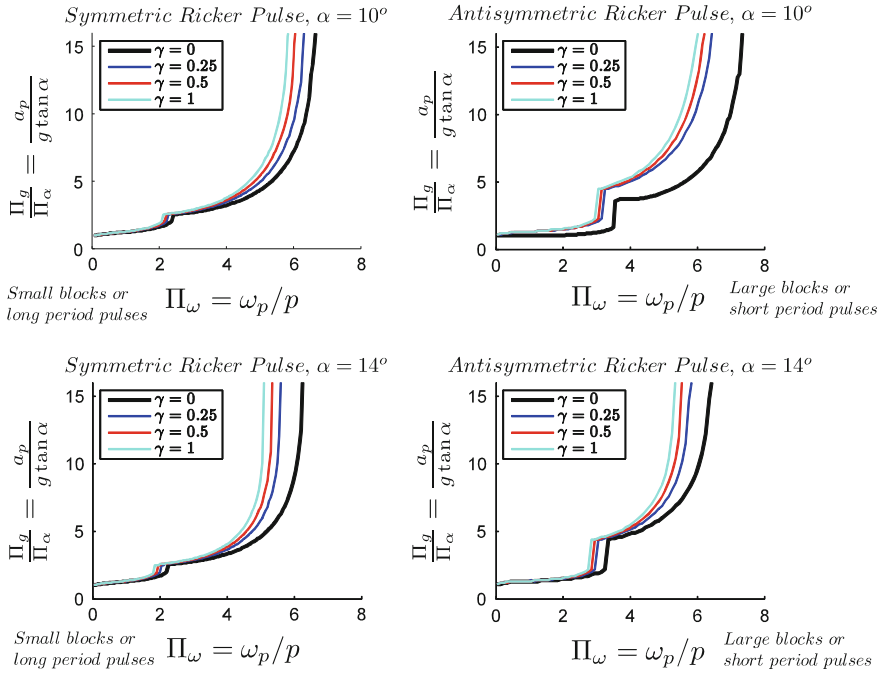


Fig. 6 Minimum overturning acceleration spectra of the free-standing rocking frame shown in Fig. 2 when subjected to a symmetric Ricker pulse (left) and an antisymmetric Ricker pulse (right) for different values of the mass ratio $\gamma = \frac{m_p}{m_c}$. Top $\alpha = 10^\circ$, Bottom $\alpha = 14^\circ$. The values of the coefficient of restitution are given by Eq. 30

5 Seismic Stability of Ancient Columns Supporting Epistyles and the Frieze Atop

In ancient Greek temples the epistyles are positioned from the vertical axis of one column to the vertical axis of the neighboring column; therefore, the joint of the epistyles are along the vertical axis of the column (see Fig. 2). With this configuration during lateral loading of the peristyle of the temple, each epistyle in addition to the horizontal translation, u , shown in Fig. 3 it will also experience a small rotation; while the transfer of forces from the epistyles to the columns is not concentrated at the top pivoting point of the columns. Nevertheless, the tendency of the epistyle to rotate is partially prevented from the friction that develops along the interface with the neighboring high-profile epistyle and the heavy stone of the frieze atop which goes over the joint of the epistyles. According to this construction pattern with very tight joints the ancient builders constructed a nearly continuous and massive structure atop the columns which according to this study enhanced appreciably the seismic-rocking stability of the peristyle of the temples. It is worth

mentioning that the numerical study of Papaloizou and Komodromos [37] concludes to the same result—that the planar response of free-standing rocking frames is more stable than the response of their solitary free-standing columns.

Two of the strongest ground motions recorded in Greece are the 1973 Lefkada record and the 1995 Aigion record [52]. Both records exhibit distinguishable acceleration pulses with durations $T_p \approx 0.6$ s. We concentrate on the Temple of Apollo in Corinth where its $7.5 \text{ m} \times 1.8 \text{ m}$ monolithic columns remain standing since 540BC in an area with high seismicity. The dimensions of its columns yield a frequency parameter $p = \sqrt{\frac{3g}{4R}} = 1.4 \text{ rad/s}$ and a slenderness $\alpha = \tan^{-1}(b/h) = 13.5^\circ$. By taking the pulse duration $T_p = 0.6$ s of the nearby Aigion record, the dimensionless term Π_ω assumes the value $\frac{\omega_p}{p} = \frac{2\pi}{pT_p} = 7.5$. For such large value of $\omega_p/p \approx 7.5$ the bottom plots of Fig. 6 give for the solitary free-standing column ($\gamma = 0$ line) an overturning ground acceleration $a_p > 15g \tan \alpha = 15g \times 0.24 = 3.6g$ —which is an unrealistically high acceleration. Consider now the extreme situation for Greece, where the predominant pulse of the ground shaking exhibits a period $T_p = 0.9$ s. A pulse period $T_p = 0.9$ s may be a rare event for the fault size and earthquake magnitude that prevail in Greece; nevertheless, it helps one understanding the appreciable seismic stability of rocking structures.

With $T_p = 0.9$ s and $p = 1.4 \text{ rad/s}$, $\omega_p/p = 5$ and according to the bottom plots of Fig. 6 which are for slenderness $\alpha = 14^\circ$, the minimum overturning acceleration of a rocking frame with $\gamma = 0.25$ exceeds the value of $a_p \approx 5g \times 0.24 = 1.2g$. This analysis shows that the free-standing peristyles of ancient temples can survive acceleration pulses as long as 0.9 s and as intense as 1.2g. While this is a physically realizable pulse [20], it is an unlikely strong shaking for the seismicity of Greece that apparently never happened over the 2500 years of the lifespan of the temple shown in Fig. 2.

6 Rocking Isolation of Bridges—Proof of Concept

The concept of allowing the piers of bridges to rock is not new. For instance, the beneficial effects that derive from uplifting and rocking have been implemented since the early 1970s in the South Rangitikei bridge in New Zealand [6]. During the last decade, the benefits /challenges associated with the rocking of bridge piers have been receiving increasing attention partly because of growing interest in the prefabricated bridge technology ([56, 43, 10] and references reported therein) and partly because of the need for the bridge structure to recenter after a strong seismic event ([9, 25, 46] among others).

In the prefabricated bridge technology the bridge piers and the deck are not free standing. The structural system is essentially a hybrid system (see [9, 56]) where the bridge pier is connected to its foundation and at the deck with a post-tensioned tendon that passes through the axis of the column together with longitudinal mild

steel reinforcement which runs near the circumference of the column. During earthquake loading the majority of deformation is concentrated at the pier-foundation and pier-cap-beam interfaces and the overall deformation pattern of the post-tensioned pier-cap-beam system resembles the deformation pattern of the free-standing rocking frame that is under investigation in this study. Nevertheless, the post-tensioning tendons and the mild-steel longitudinal reinforcement that extends into the foundation and the cap-beam contributes appreciably to the lateral moment capacity of the system and in most prefabricated bridge applications, the moment-rotation curve of the hybrid systems follows a positive slope.

Within the context of a proof-of-concept, in this study we present the planar rocking response of a free-standing two-column bridge bent where its moment rotation curve follows a negative slope given that the frame is entirely free to rock. Figure 7 shows schematically the free-standing two-column bridge bent of interest in its deformed configuration. Sliding at the pivot point during impact is prevented with a recess at the pile-cap and the cap-beam as shown in Fig. 7. In this numerical application the cylindrical piers of the free-standing bridge bent are 9.6 m tall with a diameter $d = 2b = 1.6$ m. These are typical dimensions of bridge piers for highway overpasses and other bridges in Europe and USA. Taller bridge piers will result to even more stable configurations. With $2h = 9.6$ m and $2b = 1.6$ m, the slenderness of the bridge pier is $\tan \alpha = \frac{1}{6} = 0.166$ and its frequency parameter $p = 1.23$.

Depending on the length of the adjacent spans and the per-length weight of the deck, the mass ratio $\gamma = \frac{m_b}{2m_c}$ assumes values from 4 and above ($\gamma > 4$). The larger the value of γ (heavier deck), the more stable is the free standing rocking frame (see Fig. 6). The seismic response analysis of the rocking frame has been studied until this section by using ground excitation acceleration that are pulses described either by symmetric or antisymmetric Ricker wavelets. The acceleration amplitude, a_p , and the duration, T_p , of any distinct acceleration pulse allow the use of the

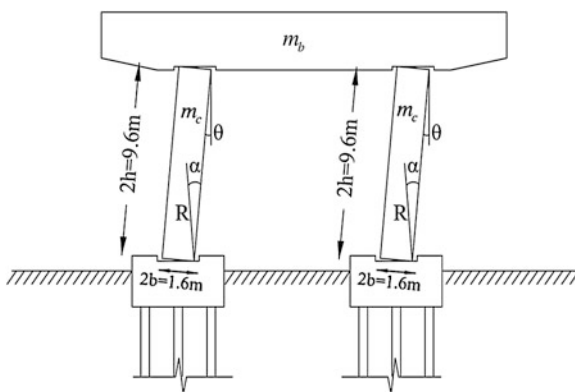


Fig. 7 Free standing rocking bridge bent. Potential sliding during impact is prevented with the recess shown. No vertical post-tensioning, no continuation of the longitudinal reinforcement of the columns through the rocking interfaces at the pile-caps and the cap-beam

dimensional analysis presented in this work and the derivation of the associated Π -products which improve the understanding of the physics that govern the problem together with the organization and presentation of the response. Nevertheless, in order to stress the main finding of this study—that top-heavy free-standing rocking frames enjoy ample seismic stability—we examine the planar seismic response of the free standing two column bridge bent shown in Fig. 7 when subjected to six strong-motion historic records listed in Table 1. The values of the acceleration amplitude, a_p , and pulse period, T_p , shown in last two columns of Table 1 have been determined with the extended wavelet transform [52].

Figure 8 plots the time histories of the normalized rotation, θ/α , together with the vertical uplift, $v(t)$, and the horizontal drift, $u(t)$, of the free standing rocking bridge bent shown in Fig. 7 with $\gamma = \frac{m_b}{2m_c} = 4$. Note that for all six strong ground motions selected in this analysis the frame rotation, θ , is less than $1/3$ of the slenderness, α , of the columns ($\theta/\alpha < 0.33$); therefore the free-standing rocking frame exhibits ample seismic stability.

The peak horizontal displacement u_{\max} ranges from 20 to 50 cm; while the vertical uplift is as high as 5 cm. The evaluation of these response quantities shall be conducted in association with the equivalent response quantities from vertically post-tensioned hybrid frames [9, 43, 56] and seismically isolated decks ([7, 11, 27, 28] among others) after considering the effects of the end-conditions of the deck at the abutments. This comparison/evaluation is the subject of an ongoing study which also examines other practical issues such as the effect of the crushing of the pivoting points of the columns [44, 45, 47] and the accommodation of the deck uplift at the end-abutments.

The main conclusion of this study is that heavy decks freely supported on free-standing piers exhibit ample seismic stability and that the heavier is the deck (even if the center of gravity rises) the more stable is the rocking frame. This conclusion may eventually lead to the implementation of the free-standing rocking frame—a

Table 1 Earthquake records used for the seismic response analysis of the free-standing rocking bridge bent

Earthquake	Record	Magnitude (Mw)	Epicentral distance (km)	PGA (g)	PGV (m/s)	a_p (g)	T_p (s)
1966 Parkfield	CO2/065	6.1	0.1	0.48	0.75	0.41	0.6
1971 San Fernando	Pacoima Dam/164	6.6	11.9	1.23	1.13	0.38	1.27
1986 San Salvador	Geotech Investig. Center	5.4	4.3	0.48	0.48	0.34	0.8
1992 Erzincan	Erzincan/EW	6.9	13	0.50	0.64	0.34	0.9
1994 Northridge	Jensen Filter Plant/022	6.7	6.2	0.57	0.76	0.39	0.5
1995 Kobe	Takarazuka/000	6.9	1.2	0.69	0.69	0.50	1.1

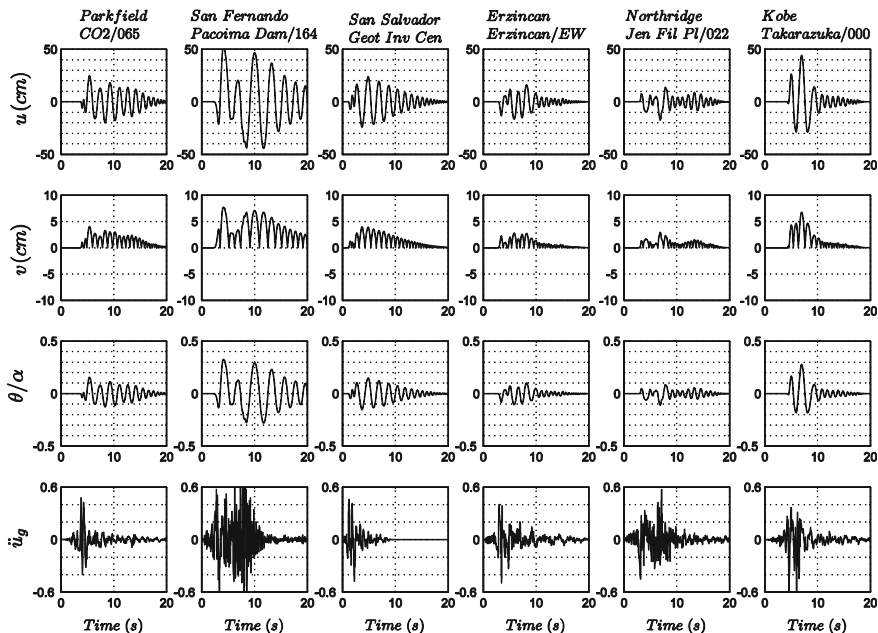


Fig. 8 Rotation, vertical and horizontal displacement histories of the free standing rocking frame shown in Fig. 7 ($p = 1.23$, $\tan \alpha = 1/6$, $\gamma = 4$) when subjected to the recorded ground motions listed in Table 1 and plotted at the *bottom*

structural configuration where all the issues associated with seismic connections such as buckling and fracture of the longitudinal reinforcing bars or spalling of the concrete cover [9, 10, 43, 46, 56] are removed as they are not an issue in the ancient temples shown in Fig. 2.

7 Conclusions

This paper investigated the planar rocking response of an array of free-standing columns capped with a freely supported rigid beam. Following a variational formulation, the paper concludes to the remarkable result that the dynamic rocking response of an array of free standing columns capped with a rigid beam is identical to the rocking response of a single free standing column with the same slenderness as the slenderness of the columns of the rocking frame; yet with larger size and more energy loss during impacts. A larger size rocking column corresponds to a more stable configuration; therefore, the presence of the freely supported cap-beam renders the rocking frame more stable despite the rise of the center of gravity.

Most importantly, the study shows that the heavier the freely supported cap-beam is, the more stable is the rocking frame implying that top-heavy rocking

frames are more stable than when they are top-light. The stability of the rocking frame is independent of the number of columns and depends only on the ratio of the weight that is transferred to the column to the weight of the column together with the size and the slenderness of the columns.

The acceleration needed to create uplift of the rocking frame is independent of the mass and the height of the center of gravity of the cap-beam and depends only on the slenderness, α , of the columns $\left(u_g^{up} = g \tan \alpha\right)$.

The findings above render rocking isolation a most attractive alternative for the seismic protection of bridges given that the heavier is the deck the more stable is the rocking bridge. The future implementation of a truly rocking frame where there is neither post-tensioning nor continuation of the longitudinal reinforcement through the rocking interfaces shall remove several of the concerns associated with the seismic connections of prefabricated bridges such as buckling and fracture of the longitudinal reinforcing bars or spalling of the concrete cover.

Acknowledgements Financial support for this study has been provided by the research project “Seismic Rock Bridge” which is implemented under the “ARISTEIA” action of the “OPERATIONAL PROGRAMME EDUCATION AND LIFELONG LEARNING” and is co-funded by the European Union (European Social Fund) and Greek National Resources.

References

1. Acikgoz S, DeJong MJ (2012) The interaction of elasticity and rocking in flexible structures allowed to uplift. *Earthq Eng Struct Dyn* 41(15):2177–2194
2. Alavi B, Krawinkler H (2001) Effects of near-source ground motions on frame-structures. Technical report No. 138, The John A. Blume Earthquake Engineering Center, Stanford University
3. Ambraseys N, Psycharis IN (2011) Earthquake stability of columns and statues. *J Earthq Eng* 15(5):685–710
4. Apostolou M, Gazetas G, Garini E (2007) Seismic response of slender rigid structures with foundation uplift. *Soil Dyn Earthq Eng* 27:642–654
5. Aslam M, Scalise DT, Godden WG (1980) Earthquake rocking response of rigid bodies. *J Struct Div ASCE* 106(2):377–392
6. Beck JL, Skinner RI (1974) The seismic response of a reinforced concrete bridge pier designed to step. *Earthq Eng Struct Dyn* 2:343–358
7. Buckle IG, Constantinou MC, Diclali M, Chasemi H (2006) Seismic isolation of highway bridges. Research report MCEER-06-SP07, MCEER, University of Buffalo, NY
8. Chen YH, Liao WH, Lee CL, Wang YP (2006) Seismic isolation of viaduct piers by means of a rocking mechanism. *Earthq Eng Struct Dyn* 35(6):713–736
9. Cheng CT (2008) Shaking table tests of a self-centering designed bridge substructure. *Eng Struct* 30:3426–3433
10. Cohagen L, Pang JBK, Stanton JF, Eberhard MO (2008) A precast concrete bridge bent designed to recenter after an earthquake. Research report, Federal Highway Administration
11. Constantinou MC, Soong TT, Dargush GF (1998) Passive energy dissipation systems for structural design and retrofit. In: Monograph series, MCEER, University of Buffalo, NY
12. Dimitrakopoulos EG, DeJong MJ (2012) Revisiting the rocking block: closed-form solutions and similarity laws. *Proc Royal Soc A Math Phys Eng Sci* 468(2144):2294–2318

13. Hall JF, Heaton TH, Halling MW, Wald DJ (1995) Near-source ground motion and its effects on flexible buildings. *Earthq Spectra* 11(4):569–605
14. Hogan, SJ (1989). On the dynamics of rigid-block motion under harmonic forcing. *Proc Royal Soc Lond A* 425:441–476
15. Hogan SJ (1990) The many steady state responses of a rigid block under harmonic forcing. *Earthq Eng Struct Dyn* 19(7):1057–1071
16. Housner GW (1963) The behaviour of inverted pendulum structures during earthquakes. *Bull Seismol Soc Am* 53(2):404–417
17. Karavasilis TL, Makris N, Bazeos N, Beskos DE (2010) Dimensional response analysis of multistorey regular steel MRF subjected to pulslike earthquake ground motions. *J Struct Eng* 136(8):921–932
18. Kirkpatrick P (1927) Seismic measurements by the overthrow of columns. *Bull Seismol Soc Am* 17(2):95–109
19. Konstantinidis D, Makris N (2005) Seismic response analysis of multidrum classical columns. *Earthq Eng Struct Dyn* 34(10):1243–1270
20. Loh CH, Lee ZK, Wu TC, Peng SY (2000) Ground motion characteristics of the Chi-Chi earthquake of 21 September 1999. *Earthq Eng Struct Dyn* 29:867–897
21. Makris N (1997) Rigidity–plasticity–viscosity: can electrorheological dampers protect base-isolated structures from near-source ground motions? *Earthq Eng Struct Dyn* 26:571–591
22. Makris N (2014) The role of rotational inertia on the seismic resistance of free-standing rocking columns and articulated frames. *Bull Seismol Soc Am* 104(5):22226–22239
23. Makris N, Chang SP (2000) Effect of viscous, viscoplastic and friction damping on the response of seismic isolated structures. *Earthq Eng Struct Dyn* 29(1):85–107
24. Makris N, Roussos Y (2000) Rocking response of rigid blocks under near-source ground motions. *Geotechnique* 50(3):243–262
25. Makris N, Zhang J (2004) Seismic response analysis of highway overcrossings equipped with elastomeric bearings and fluid dampers. *J Struct Eng ASCE* 130(6):830–845
26. Makris N, Konstantinidis D (2003) The rocking spectrum and the limitations of practical design methodologies. *Earthq Eng Struct Dyn* 32:265–289
27. Makris N, Black CJ (2004) Dimensional analysis of rigid-plastic and elastoplastic structures under pulse-type excitations. *J Eng Mech (ASCE)* 130(9):1006–1018
28. Makris N, Black CJ (2004) Dimensional analysis of bilinear oscillators under pulse-type excitations. *J Eng Mech (ASCE)* 130(9):1019–1031
29. Makris N, Psychogios C (2006) Dimensional response analysis of yielding structures with first-mode dominated response. *Earthq Eng Struct Dyn* 35:1203–1224
30. Makris N, Vassiliou MF (2012) Sizing the slenderness of free-standing rocking columns to withstand earthquake shaking. *Arch Appl Mech* 82(10–11):1497–1511
31. Makris N, MF Vassiliou (2013) Planar rocking response and stability analysis of an array of free-standing columns capped with a freely supported rigid beam. *Earthq Eng Struct Dyn* 42(3):431–444
32. Makris N, Vassiliou MF (2014) Are some top-heavy structures more stable? *J Struct Eng* 140(5)
33. Mavroeidis GP, Papageorgiou AS (2003) A mathematical representation of near-fault ground motions. *Bull Seism Soc Am* 93(3):1099–1131
34. Milne J (1885) Seismic experiments. *Trans Seism Soc Jpn* 8:1–82
35. Palmeri A, Makris N (2008) Response analysis of rigid structures rocking on viscoelastic foundation. *Earthq Eng Struct Dyn* 37:1039–1063
36. Palmeri A, Makris N (2008) Linearization and first-order expansion of the rocking motion of rigid blocks stepping on viscoelastic foundation. *Earthq Eng Struct Dyn* 37:1065–1080
37. Papaloizou L, Komodromos K (2009) Planar investigation of the seismic response of ancient columns and colonnades with epistyles using a custom-made software. *Soil Dyn Earthq Eng* 29(11–12):1437–1454
38. Pecker A (2005) Design and construction of the foundations of the Rion Antirion Bridge. In *Proceedings of the 1st Greece–Japan workshop on seismic design, observation, retrofit of foundations*, Athens (pp 119–130)

39. Psycharis IN, Jennings PC (1983) Rocking of slender rigid bodies allowed to uplift. *Earthq Eng Struct Dyn* 11:57–76
40. Prieto F, Lourenço PB, Oliveira CS (2004) Impulsive Dirac-delta forces in the rocking motion. *Earthq Eng Struct Dyn* 33:839–857
41. Ricker N (1943) Further developments in the wavelet theory of seismogram structure. *Bull Seismol Soc Am* 33:197–228
42. Ricker N (1944) Wavelet functions and their polynomials. *Geophysics* 9:314–323
43. Pang JBK, Stenk KP, Cohagen L, Stanton JF, Eberhard MO (2008) Rapidly constructible large-bar precast bridge-bent seismic connection. In: Research Report WA-RD684.2, Washington State Department of Transportation
44. Roh H, Reinhorn A (2010) Nonlinear static analysis of structures with rocking columns. *J Struct Eng ASCE* 136(5):532–542
45. Roh H, Reinhorn A (2010) Modeling and seismic response of structures with concrete rocking columns and viscous dampers. *Eng Struct* 32:2096–2107
46. Sakai J, Hyungil J, Mahin S (2006) Reinforced concrete bridge columns that re-center following earthquakes. In: Proceedings of the 8th US National Conference on Earthquake Engineering, April 18–22, San Francisco, California
47. Skinner RI, Beck JL, Bycroft GN (1974) A practical system for isolating structures from earthquake attack. *Earthq Eng Struct Dyn* 3(3):297–309
48. Sharpe RD, Skinner RI (1983) The seismic design of an industrial chimney with rocking base. *Bulletin*, New Zealand
49. Spanos, PD, Koh AS (1984) Rocking of rigid blocks due to harmonic shaking. *J Eng Mech ASCE* 110(11):1627–1642
50. Truniger R, Vassiliou MF, Stojadinovic B. (2014) Experimental study on the interaction between elasticity and rocking. In: Proceedings of the 10th national conference in earthquake engineering, Earthquake Engineering Research Institute, Anchorage, AK
51. Vassiliou M, Makris N (2009) Evaluation of the coherence of strong ground motions using wavelet analysis. In: ACES workshop: advances in performance-based earthquake engineering, Corfu, Greece, July 4–7
52. Vassiliou MF, Makris N (2011) Estimating time scales and length scales in pulselike earthquake acceleration records with wavelet analysis. *Bull Seismol Soc Am* 101(2):596–618
53. Vassiliou MF, Makris N (2012) Analysis of the rocking response of rigid blocks standing free on a seismically isolated base. *Earthq Eng Struct Dyn* 41(2):177–196
54. Vassiliou MF, Mackie KR, Stojadinović B (2014) Dynamic response analysis of solitary flexible rocking bodies: modeling and behavior under pulse-like ground excitation. *Earthq Eng Struct Dyn* 43:1463–1481
55. Veletsos AS, Newmark NM, Chelepati CV (1965) Deformation spectra for elastic and elastoplastic systems subjected to ground shock and earthquake motions. In: Proceedings of the 3rd world conference on earthquake engineering, vol II. Wellington, New Zealand, pp 663–682
56. Wacker JM, Hieber DG, Stanton JF, Eberhard MO (2005) Design of precast concrete piers for rapid bridge construction in seismic regions. Research Report, Federal Highway Administration
57. Yim CS, Chopra AK, Penzien J (1980) Rocking response of rigid blocks to earthquakes. *Earthq Eng Struct Dyn* 8(6):565–587
58. Zhang J, Makris N (2001) Rocking response of free-standing blocks under cycloidal pulses. *J Eng Mech ASCE* 127(5):473–483

Seismic Assessment, Behavior and Retrofit of Heritage
Buildings and Monuments

Psycharis, I.N.; Pantazopoulou, S.J.; Papadrakakis, M.
(Eds.)

2015, XI, 490 p. 333 illus., 239 illus. in color., Hardcover

ISBN: 978-3-319-16129-7